Research Square

Preprints are preliminary reports that have not undergone peer review.
They should not be considered conclusive, used to inform clinical practice,
or referenced by the media as validated information.

Complexity synchronization networks reveal distinct modes of coordination in an adaptive predator–prey model

Korosh Mahmoodi

korosh.mahmoodi@gmail.com

U.S. Army Combat Capabilities Development Command Armaments Center

Scott E. Kerick

U.S. Army Combat Capabilities Development Command Armaments Center

Piotr J. Franaszczuk

U.S. Army Combat Capabilities Development Command Armaments Center

David L. Boothe

U.S. Army Combat Capabilities Development Command Armaments Center

Paolo Grigolini

University of North Texas

Bruce J. West

University of North Texas

Article

Keywords:

Posted Date: November 25th, 2026

DOI: https://doi.org/10.21203/rs.3.rs-11598619/v1

License: This work is licensed under a Creative Commons Attribution 4.0 International License.
Read Full License

Additional Declarations: No competing interests reported.

Complexity synchronization networks reveal distinct modes of coordination in an adaptive predator–prey model

Korosh Mahmoodi[1,*], Scott E. Kerick[1], Piotr J. Franaszczuk[1], David L. Boothe[1], Paolo Grigolini[2], and Bruce J. West[2]

[1]U.S. Army Combat Capabilities Development Command Army Research Laboratory, Aberdeen Proving Ground, MD 21005, USA
[2]Center for Nonlinear Science, University of North Texas, Denton, TX 76203, USA
[*]korosh.mahmoodi@gmail.com

ABSTRACT

Complexity synchronization (CS) networks track how the scaling properties of interacting signals evolve together, offering a view of coordination beyond the trajectories themselves. We explore this approach in an adaptive predator–prey model in which two predators learn when to exchange information, trust one another, and share payoffs. From the evolving decision thresholds, we construct CS networks using modified diffusion entropy analysis (MDEA) and detrended fluctuation analysis (DFA). The two approaches reveal strikingly different relationships with cooperative performance: MDEA-based CS increases with cooperation across the sensing conditions examined, whereas DFA-based CS decreases. Across ten independent stochastic ensembles, the opposite cooperation–CS slopes are reproduced for three threshold pairs (six Holm-adjusted tests, $p = 0.0084$; ensemble-bootstrap 95% confidence intervals exclude zero). We then examine how the networks reorganize when payoff-sharing learning is weakened and subsequently restored. Comparing three equal-budget interventions illustrates how network-level descriptions can accompany changes in cooperative function and help motivate targeted studies of recovery. Together, these results establish estimator-dependent CS networks as a promising framework for examining the temporal organization of adaptive cooperation.

Introduction

Cooperation is not an obvious outcome when individuals act in their own interest. The Prisoner's Dilemma makes the tension particularly clear: an action that benefits an individual in the short term can undermine the pair's longer-term success. Repeated interaction and adaptation can nevertheless support cooperation[1,2]. In a moving predator–prey setting, the problem becomes more concrete. Two predators must decide what to share and whom to trust while the prey continually changes the information available to them.

Most descriptions of coordination begin with the observed signals. Correlation captures covariation in their values; phase synchronization captures alignment of oscillatory timing[3,4]. Neither description directly addresses whether the statistical character of a signal changes in concert with that of another. That distinction can matter in adaptive systems, whose behavior may alternate between relatively persistent and more intermittent episodes. Coordinated physiological and interpersonal activity provides a broader motivation for studying such time-varying organization[5,6].

Complexity synchronization (CS) was introduced to describe covariation between local scaling exponents rather than between the original signal values. Previous work reported this behavior in physiological networks[7,8]. The present question is different. Can this form of coordination be related to a measurable behavioral outcome when the underlying variables are adaptive decisions, rather than physiological recordings? And does the answer depend on how the scaling exponent is estimated?

The second question is important because different scaling methods need not respond to the same temporal structure. Modified diffusion entropy analysis (MDEA) constructs a diffusion process from detected events; detrended fluctuation analysis (DFA) characterizes fluctuations and their correlations in the original record. Intermittent, potentially renewal-like events are one source of anomalous scaling[9], but persistent correlations can also produce scaling. We therefore compare the two approaches rather than treating their estimates as interchangeable measures of an underlying "amount of complexity."

We use a reduced version of the Selfish Algorithm framework[10]. Two predators adapt thresholds for information sharing, trust, and payoff sharing while pursuing a prey that introduces uncertainty into their observations. This

gives us both a behavioral outcome—cooperation—and six evolving internal variables from which to construct CS networks. By varying the sensing radius, we can examine how the relationship between cooperation and scaling coordination changes across interaction conditions.

A second set of experiments concerns recovery after a known perturbation. Work on network control and resilience has shown why the choice of intervention can matter as much as its overall magnitude[11–13]. Here we reduce the learning increments of both payoff-sharing thresholds and compare their direct restoration with two alternatives that use the same total adjustment. By following both cooperation and the CS network through damage and recovery, we can explore how changes in adaptive performance appear in the temporal coordination structure.

An ensemble-level analysis also tests whether the estimator-dependent relationships recur across independent stochastic realizations rather than relying on nominal significance from overlapping windows. The contribution is therefore twofold. First, we show that the relationship between cooperation and scaling coordination changes with the estimator: MDEA- and DFA-based CS have contrasting associations with performance in this model. Second, we place the evolving CS networks alongside a controlled damage-and-recovery experiment. Previous physiological CS studies did not test this particular link to adaptive strategic behavior; conventional signal synchronization and complexity matching address different observables; and the intervention comparison concerns adaptive learning channels rather than driver nodes in a fixed graph. Together, these analyses extend CS from physiological recordings to adaptive decision dynamics and show how network representations can be used to investigate cooperative organization and recovery.

Methods

Reduced Predator–Prey model

We study a minimal adaptive multi-agent system consisting of two Predator agents and one Prey agent moving on a two-dimensional domain with periodic boundary conditions (Fig. 1). The Predators represent the potentially cooperative elements of the system, while the Prey provides a dynamic and partially unpredictable environment that continuously reshapes the interaction.

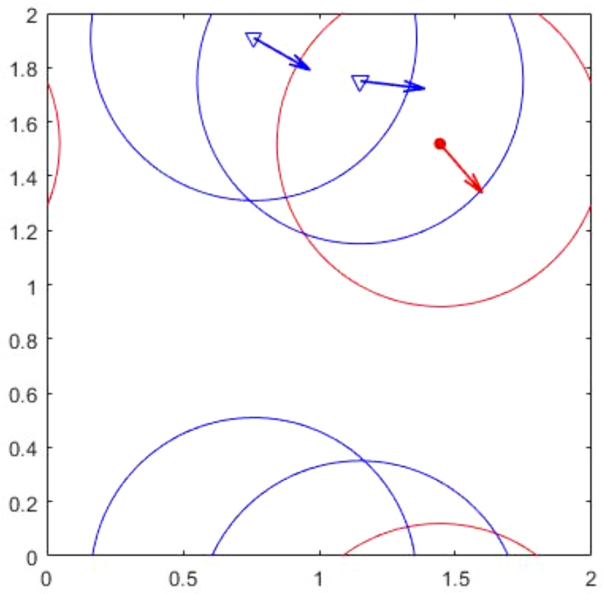


Figure 1. Reduced Predator–Prey environment. Two Predator agents and one Prey move on a two-dimensional periodic domain. Sensing radii define local interaction neighborhoods, and the agents update their headings according to the adaptive decision rules described in the text.

Environment and sensing Each agent interacts with its surroundings through a finite sensing (vision) radius r_S, defining the set of neighboring agents it can detect at each time step. For parameter sweeps, we use the dimensionless sensing-radius ratio $R = r_S/L$, where L is the side length of the square domain; thus $r_S = R \times L$. Based on this local information, agents estimate target directions and update their motion on the periodic domain.

Adaptive decision dynamics Each Predator is characterized by three internal adaptive variables associated with information sharing, trust, and payoff sharing. These variables encode behavioral propensities and evolve over time through payoff-driven learning. At every time step, they generate probabilistic binary decisions, allowing agents to flexibly switch between alternative actions.

Interaction and information exchange Predators estimate the Prey's direction by projecting its motion based on local observations. Due to the Prey's deceptive behavior, this estimate is uncertain and can take one of two possible forms. When a Predator relies on its partner, it replaces its estimate with the complementary estimate inferred by the other Predator. This complementary exchange allows the pair to span the uncertainty in the Prey's trajectory and constitutes the primary coupling mechanism.

The Prey, in turn, anticipates the Predators' motion and selects between two symmetric evasive directions at each step. This stochastic two-option mechanism introduces intrinsic uncertainty and maintains a nonstationary environment.

Payoff and cooperation Successful capture events—determined by proximity within an interaction radius—can trigger a payoff-sharing interaction between the Predators. In this stage, agents face a Prisoner's Dilemma–like trade-off between cooperation and defection. In the implementation used here, the payoff-sharing stage is entered only if at least one Predator successfully captures the Prey and at least one trust decision is realized. Mutual cooperation is then recorded when both Predators choose to share payoff, i.e.,

$$s_1^{(P)}(t) = s_2^{(P)}(t) = 1.$$

The cooperation rate C_r is defined as the running fraction of these events (i.e., both agents decide to share payoff) over time.

This reduced model combines local sensing, adaptive internal dynamics, complementary information exchange, and a dynamically deceptive environment in a minimal setting that allows the emergence and organization of cooperation to be studied. Full implementation details are provided in the Supplementary Information.

Complexity analysis

The empirical signals analyzed in the present study are the threshold time series

$$I_1,\ T_1,\ P_1,\ I_2,\ T_2,\ P_2,$$

corresponding to information-sharing, trust, and payoff-sharing thresholds for the two Predators. We analyze the temporal complexity of these signals using modified diffusion entropy analysis (MDEA). MDEA converts each threshold trajectory into an event sequence by stripe crossing. Events are defined as crossings of equally spaced amplitude thresholds ("stripes") applied to the signal. Smaller stripe sizes increase the density of detected events and, in the limit, approach noise-dominated regimes, whereas larger stripe sizes capture coarser, more structured fluctuations.

For all reported MDEA analyses, local scaling exponents were estimated using sliding windows of length 10^4 samples with 75% overlap after removal of the first 25% of each simulation as burn-in. Three representative stripe sizes (0.1, 0.01, and 0.001) were examined. Within each window, MDEA was applied to the stripe-crossing event sequence to obtain a local scaling exponent $\delta(t)$. Repeating this procedure across overlapping windows generated the time-dependent scaling signals used for complexity-synchronization analysis.

For comparison, we also estimate scaling exponents $H(t)$ using detrended fluctuation analysis (DFA), which analyzes correlations directly in the original time series rather than through event sequences, and is therefore more sensitive to persistent long-range memory.

CS is then defined as the correlation between the resulting scaling-exponent time series. In this way, CS measures synchronization of changing statistical structure rather than synchronization of raw amplitudes.

Ensemble-level statistical validation We assessed the reproducibility of the cooperation–CS relationships using the ten stochastic ensembles as the resampling units. For each estimator and each of three prespecified threshold pairs (I_1–I_2, I_2–T_1, and I_1–P_2), a separate ordinary least-squares slope of cooperation rate against CS was calculated across the 21 sensing-radius settings within each ensemble. For MDEA, the validation script used the intermediate stripe size of 0.01; the DFA results do not have a stripe-size dimension. We summarized the ten slopes by their mean and obtained percentile 95% confidence intervals from 5,000 bootstrap samples of ensembles drawn with replacement. A two-sided Monte Carlo sign-flip test (5,000 random sign assignments, with a plus-one correction) tested the ensemble mean slope against zero under the assumption of sign exchangeability. The resulting six p-values

were adjusted by the Holm procedure. The code used a fixed random seed for reproducibility. Numerical results are provided in Supplementary Table S1 and the ensemble-level plot in Supplementary Fig. S6.

These tests avoid treating the overlapping scaling windows as independent replicates, but they do not make the sensing-radius sweep a randomized experiment, establish independence of the 21 settings within a simulation, or test causal prediction by CS. The sign-flip test also assumes the ensemble-level slopes have a distribution sufficiently symmetric under the null; the bootstrap intervals are conditional on the ten ensembles and the simulated parameter settings. The original nominal Pearson-correlation p-values on overlapping scaling windows are not used as evidence of statistical significance. Filled/open markers and solid/dashed network edges in the original figures remain legacy plotting conventions, not inferential labels. Individual CS network edges have not been subjected to this new ensemble-level significance test. Regression R^2 describes goodness of fit to plotted summaries, not out-of-sample predictive performance.

Renewal-support analysis

To provide supporting mechanistic evidence for the event-driven interpretation of the MDEA results, we also analyzed the renewal properties of stripe-crossing events. These analyses were performed as representative tests on the information-sharing threshold of Predator 1, I_1, rather than on all threshold variables or on the CS pairs directly. The goal was not to define CS, but to examine whether the event sequence extracted from an adaptive threshold exhibits renewal-like organization in the low- and high-cooperation regimes.

For the survival-function aging analysis shown in Supplementary Information, Fig. S4, the first half of each simulation was discarded, and a single window of length 10^4 samples was selected from the remaining I_1 trajectory. Stripe-crossing events were extracted using the same stripe sizes used in the MDEA analysis (0.1, 0.01, and 0.001). The inter-event interval τ was defined as the number of samples between successive crossings from one stripe to another. The aging time was fixed at $t_a = 100$, and the aged survival function was compared with a shuffled-aged control obtained by randomly permuting the inter-event intervals before applying the same aging procedure.

For the inter-event-interval autocorrelation analysis shown in Supplementary Information, Fig. S5, the first half of the I_1 trajectory was again discarded. Autocorrelations were then computed from the τ sequences extracted from 10 windows of length 10^4 samples with 75% overlap. The plotted curves show the mean autocorrelation across these windows, with variability shown as the window-to-window standard deviation. Because the autocorrelation functions can oscillate around zero, a power-law fit to the upper envelope of the absolute autocorrelation was used as a compact summary of the long-lag decay rate; more negative envelope slopes indicate faster decay of inter-event memory.

Simulation summary

The simulations reported here sweep the dimensionless sensing-radius ratio $R = r_S/L$ over 21 values, use 10 ensembles per condition, and evaluate CS for three representative stripe sizes. Each run contains 10^6 trials, with a burn-in period removed before analysis. The learning increment is fixed at $\Delta_S = 0.1$, and a small stochastic term is included in the threshold update rule. Full numerical details, ordinary-correlation control analyses, and renewal-related supporting analyses are provided in the Supplementary Information.

Perturbation and rescue protocol

To compare restoration strategies for a predefined perturbation, we applied perturbations to the learning increments of the adaptive thresholds. The threshold order used throughout the analysis is

$$(I_1, T_1, P_1, I_2, T_2, P_2).$$

The baseline learning vector is

$$\boldsymbol{\Delta}_{\text{base}} = 0.1\,(1,1,1,1,1,1),$$

whereas the damaged condition reduces the payoff-sharing learning increments for both agents,

$$\boldsymbol{\Delta}_{\text{damage}} = (0.1, 0.1, 0.025, 0.1, 0.1, 0.025).$$

Thus, the perturbation selectively weakens the adaptive channel associated with the payoff-sharing thresholds P_1 and P_2, while leaving the information-sharing and trust-related learning increments unchanged.

We compared three rescue strategies with rescue strength $s \in [0,1]$. Let $b = 0.075s$ denote the increment added to each selected channel. The implemented vectors are

$$\begin{aligned}
\boldsymbol{\Delta}_{\text{target}}(s) &= (0.1, 0.1, 0.025+b, 0.1, 0.1, 0.025+b),\\
\boldsymbol{\Delta}_{\text{local}}(s) &= (0.1+b, 0.1, 0.025, 0.1, 0.1+b, 0.025),\\
\boldsymbol{\Delta}_{\text{global}}(s) &= \boldsymbol{\Delta}_{\text{damage}} + \frac{2b}{6}(1,1,1,1,1,1).
\end{aligned}$$

Thus all strategies add the same total learning-increment budget $2b$. Targeted rescue restores the known damaged P_1–P_2 pair; the selected local control increases the healthy I_1 and T_2 increments above baseline while leaving P_1 and P_2 damaged. This is one specified non-targeted control, not an average over randomly selected targets. Global rescue distributes the budget over all six channels. At $s = 0$ all strategies coincide with damage; at $s = 1$ only targeted rescue exactly restores the baseline vector.

The healthy increments and damaged subsystem are specified in advance. The protocol tests targeted restoration in a known model; it does not establish blinded diagnosis, automatic target selection, or the superiority of CS over other target-selection measurements.

All rescue analyses use 10^6 trials and ENS = 10 independent stochastic ensembles, with distinct random seeds for each ensemble and condition.

A representative segment of the adaptive threshold dynamics used as input to the scaling analyses is shown in Fig. 2.

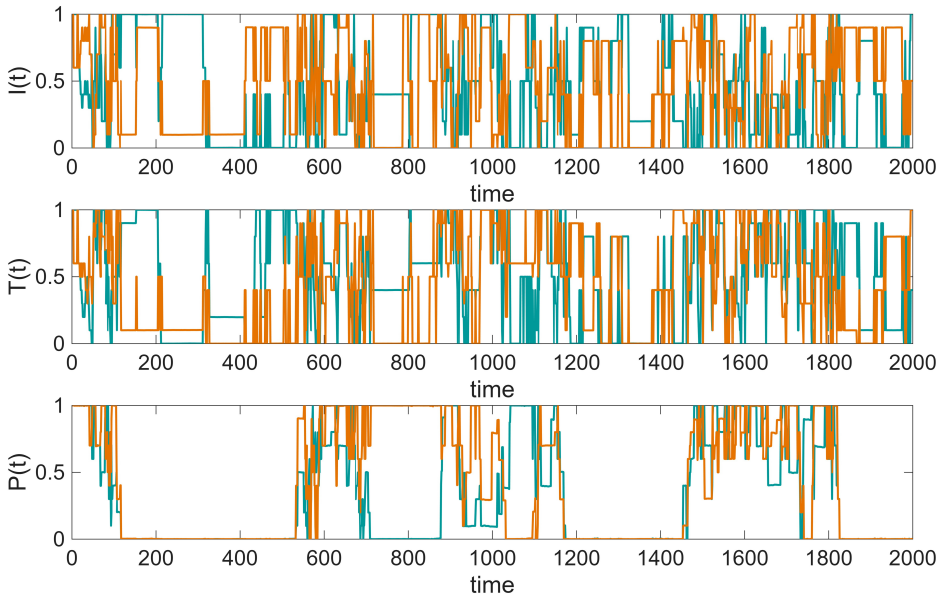


Figure 2. Representative short time series of the three adaptive threshold variables, information sharing $I(t)$, trust $T(t)$, and payoff sharing $P(t)$, over 2000 trials (out of 10^6). The two colored traces correspond to the two Predator agents. These threshold dynamics form the raw signals from which local scaling exponents are extracted using MDEA and DFA.

Results

Learning improves cooperation and payoff

Before turning to CS, we first verify that adaptive learning changes the behavioral outcome of the model. Figure 3 shows that learning increases both the cooperation rate C_r, which is the running fraction of cooperative events per trial, and the payoff rate P_r, which is the running mean payoff per trial of the predators, relative to the non-learning baseline across the dimensionless sensing-radius ratio $R = r_S/L$ (equivalently, $r_S = R \times L$; left panel), and also improves the time-resolved trajectories of these quantities in representative runs (right panel). In both panels, the curves show the average over ten simulations. This establishes that the adaptive threshold dynamics generate a meaningful cooperative regime whose temporal organization can then be analyzed using complexity-based measures.

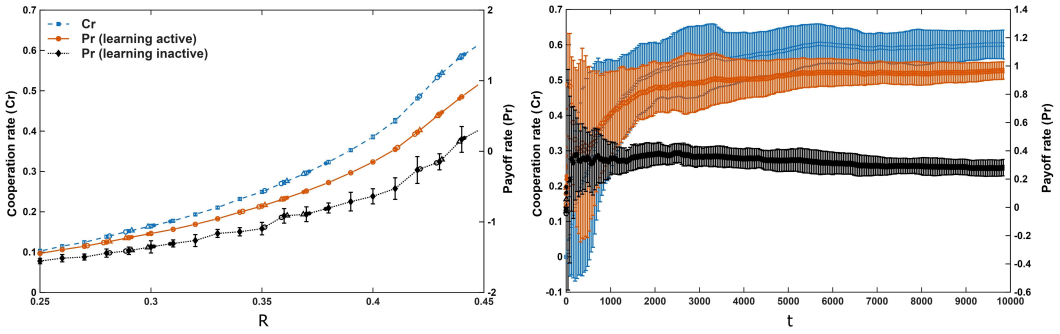


Figure 3. Performance validation of the Predator–Prey model. Left panel: Cooperation rate C_r and payoff rate P_r (at $t = 10^6$) are shown as functions of the sensing radius ratio R for simulations with learning and without learning. Right panel: time evolution of the same quantities for $R = 0.45$.

Scaling estimation from adaptive threshold dynamics

The first step in the complexity analysis is to estimate local scaling exponents from the threshold signals. Figure 4 illustrates this procedure for both MDEA and DFA. The left panels show the resulting time-dependent scaling exponents obtained from sliding windows, whereas the right panels show representative scaling plots from one selected window. These local scaling signals form the basis for the CS measures used throughout the remainder of the Results section.

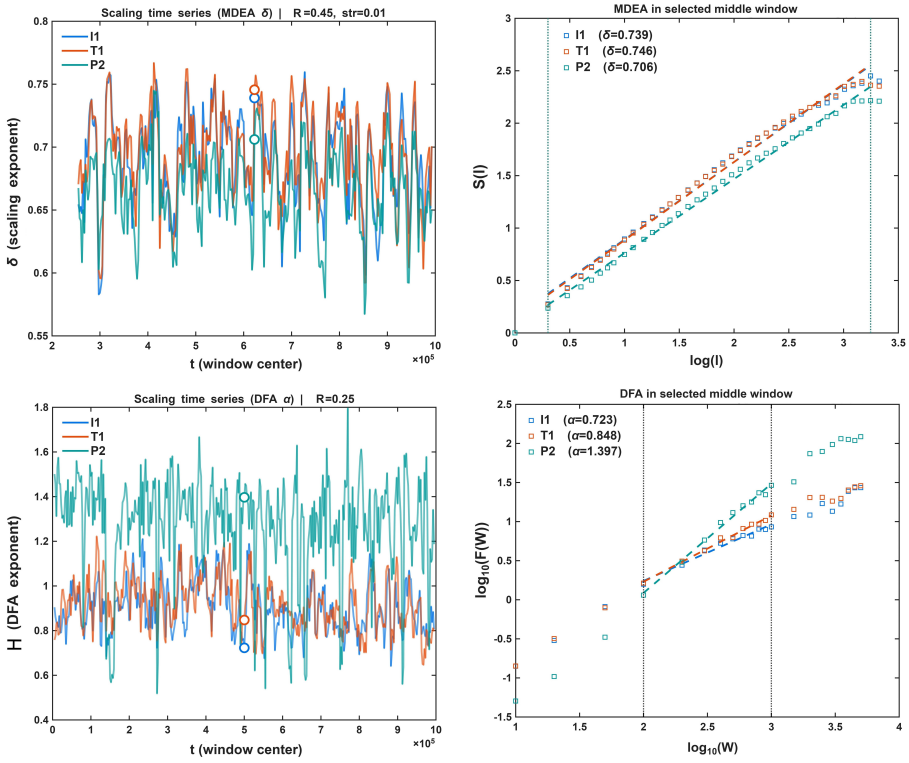


Figure 4. Example of local scaling estimation from the adaptive threshold dynamics. Left panels: scaling-exponent time series obtained from sliding windows using MDEA (top) and DFA (bottom). Right panels: the corresponding scaling plots for a selected window, marked by circles, in the left panels. In the top-right panel, the entropy $S(l)$ is plotted against $\log(l)$, where l is the length of the moving window in the MDEA; in the bottom-right panel, the fluctuation function is plotted on log–log axes, where W is the length of the moving window in the DFA. The fitted slopes define the local scaling exponents used throughout the paper. For the details of MDEA and DFA, see Supplementary Sections S4 and S5, respectively.

Cooperation and CS

A central descriptive result is the relationship between cooperative performance and estimator-specific CS. When CS is evaluated using MDEA, the cooperation rate C_r increases with synchronization of scaling dynamics (Fig. 5). In contrast, the same comparison based on DFA yields the opposite trend (Fig. 6).

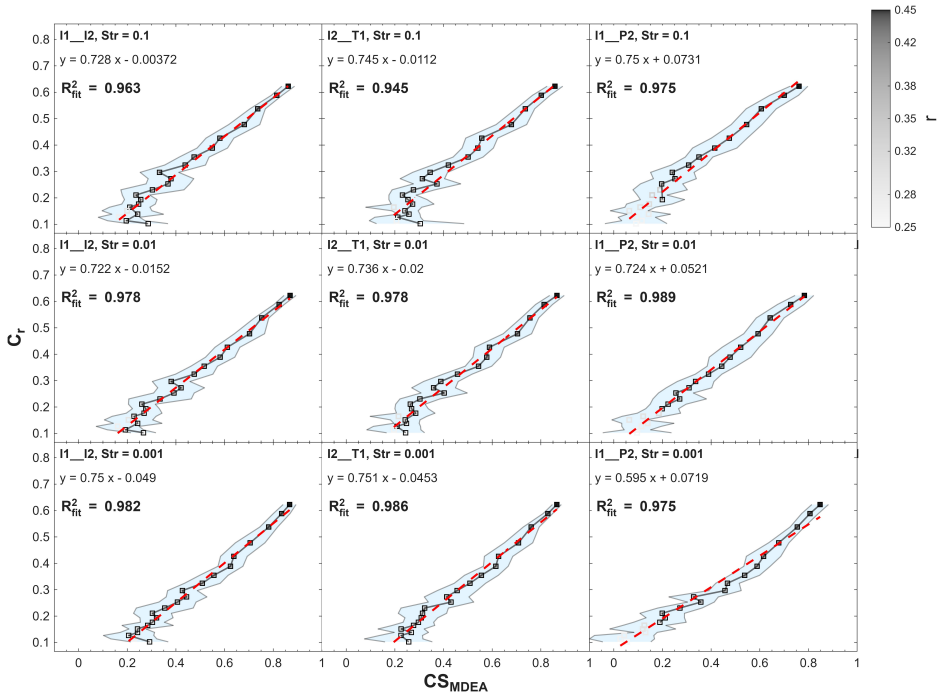


Figure 5. Relationship between cooperation rate C_r and MDEA-based CS. Columns correspond to representative threshold pairs (I_1–I_2, I_2–T_1, and I_1–P_2), and rows correspond to stripe sizes used in MDEA (Str $= 0.1, 0.01, 0.001$). Each marker represents a simulation at a different sensing ratio $R \in [0.25, 0.45]$, with grayscale indicating the R value (color bar). Filled and open squares retain the original nominal-p-value plotting convention; they are not interpreted as evidence of statistical significance. The plotted correlations and fits are descriptive (see Methods). Red dashed lines show linear fits, with corresponding regression equations and R^2_{fit} values reported in each panel. Shaded bands indicate variability across realizations (mean ± standard deviation).

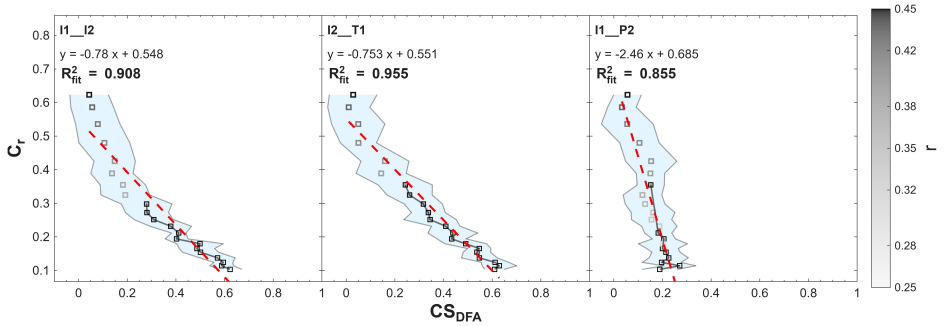


Figure 6. Relationship between cooperation rate C_r and DFA-based CS. Each panel corresponds to a representative threshold pair (I_1–I_2, I_2–T_1, and I_1–P_2), with scaling exponents estimated using detrended fluctuation analysis (DFA). Each marker represents a simulation at a different sensing ratio $R \in [0.25, 0.45]$, with grayscale indicating the R value (color bar). Filled and open squares retain the original nominal-p-value plotting convention; they are not interpreted as evidence of statistical significance. The plotted correlations and fits are descriptive (see Methods). Red dashed lines show linear fits, with corresponding regression equations and R^2_{fit} values reported in each panel. Shaded bands indicate variability across realizations (mean ± standard deviation).

Taken together, the plotted results show a positive association between cooperation and MDEA-based CS and a

contrasting negative association for DFA-based CS in the conditions examined. These are descriptive associations, not proportionality laws.

The consistency of these trends across multiple threshold pairs, stripe sizes, and interaction regimes shows that the descriptive contrast occurs across several analysis choices within this model; it is not a formal test of a universal relationship. We emphasize, however, that the sign of the DFA-based relation need not be universal across all adaptive systems. In other models, cooperation could in principle be supported by synchronized persistence, stable memory, or common slow environmental forcing, in which case a positive relation between C_r and CS_{DFA} could emerge. The distinctive result here is therefore not that DFA-based CS must always oppose cooperation, but that in the present Predator–Prey model cooperative organization is more strongly aligned with event-driven synchronization than with synchronization of persistent long-range memory. The ordinary Pearson-correlation control analysis is provided in Supplementary Information, Fig. S3.

We therefore interpret the contrast between MDEA-based and DFA-based CS not simply as a difference in predictive direction, but as a diagnostic signature of distinct coordination modes. In this sense, the point of the present analysis is not that higher CS must universally imply better performance, but that comparing different forms of CS helps identify how coordination is organized in a given adaptive system.

As a control analysis, we also examined ordinary Pearson correlations computed directly from the raw adaptive threshold signals. Supplementary Information, Fig. S3 shows the pair-specific correlations for all 15 threshold pairs as a function of the sensing-radius parameter R, together with the cooperation rate C_r. This analysis separates conventional linear similarity among the raw variables from synchronization of the time-dependent scaling dynamics used to define CS. While some threshold pairs exhibit substantial raw correlations, these correlations are highly pair-specific and summarize a different aspect of the signals; this comparison does not test which representation better selects intervention targets.

Ensemble-level validation of the cooperation–CS contrast

To test whether the opposite trends in Figs. 5 and 6 recur across stochastic realizations, we estimated the cooperation-versus-CS slope separately in each of ten ensembles over the sensing-radius sweep. For the intermediate MDEA stripe size (0.01), the mean slopes were 0.633 for I_1–I_2, 0.654 for I_2–T_1, and 0.666 for I_1–P_2. Their respective 95% ensemble-bootstrap intervals were $[0.609, 0.658]$, $[0.638, 0.669]$, and $[0.648, 0.685]$. For DFA, the corresponding mean slopes were -0.698, -0.684, and -1.250, with intervals $[-0.738, -0.659]$, $[-0.720, -0.649]$, and $[-1.354, -1.145]$. Each of the six two-sided sign-flip tests yielded a Holm-adjusted $p = 0.0084$ (Supplementary Table S1; Supplementary Fig. S6).

The consistency across independent ensembles strengthens the central observation: event-based and fluctuation-based CS networks capture different relationships between temporal coordination and cooperative performance in this model.

Renewal-related supporting analyses

To further interpret the temporal mechanism underlying the observed complexity-synchronization patterns, we examined stripe-crossing events extracted from the representative information-sharing threshold of Predator 1, I_1. The renewal aging test (Supplementary Information, Fig. S4) compares survival functions, aged survival functions, and shuffled-aged controls after discarding the first half of the simulation and analyzing one window of length 10^4 samples. The inter-event autocorrelation analysis (Supplementary Information, Fig. S5) uses 10 overlapping windows of length 10^4 samples and quantifies memory in the inter-event interval sequence $\{\tau_i\}$. These analyses are supporting mechanistic evidence rather than additional definitions of CS. They suggest that the high-cooperation regime is accompanied by weaker inter-event memory and a closer approximation to renewal-like event organization, consistent with the positive relationship between MDEA-based CS and cooperation shown in Fig. 5.

CS patterns under perturbation and restoration

The pairwise structure of CS defines a descriptive network over the interacting components of the system. Each pairwise CS value can be interpreted as the strength of alignment between the evolving scaling dynamics of two adaptive variables. In this view, CS is not a single global quantity, but a distributed field that reveals how coordination is organized across information sharing, trust, and payoff sharing.

CS tracks regime-dependent changes in cooperation We first examined how CS varies with the learning strength k of the payoff-sharing thresholds across different sensing regimes. Figure 7 shows that MDEA-based CS exhibits a clear dependence on k, with a strong contrast between low- and high-cooperation regimes. For $R = 0.25$, CS remains weak across threshold pairs and varies only modestly with k. For $R = 0.45$, CS increases sharply and organizes into

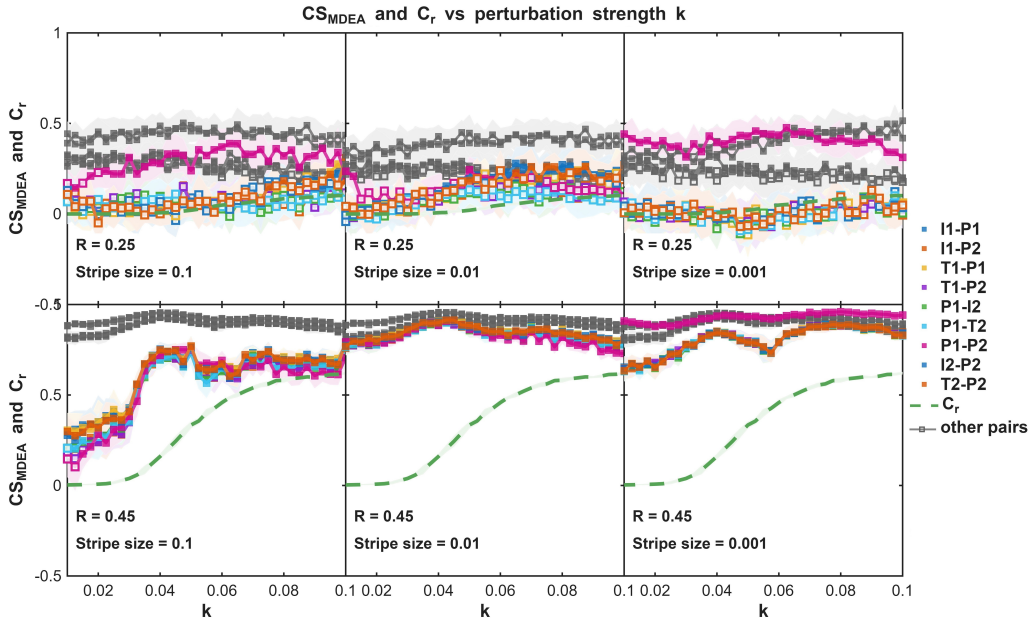


Figure 7. CS, computed using modified diffusion entropy analysis (MDEA), and cooperation rate (C_r) as functions of learning strength k of the SharePay thresholds. The top row corresponds to $R = 0.25$ and the bottom row to $R = 0.45$. Columns represent stripe sizes of 0.1, 0.01, and 0.001, respectively. Colored curves denote CS between selected threshold pairs (I, T, P) involving the payoff sharing thresholds, while gray curves represent other pairwise combinations. The dashed green curve indicates the corresponding C_r. Shaded regions denote variability across ensembles.

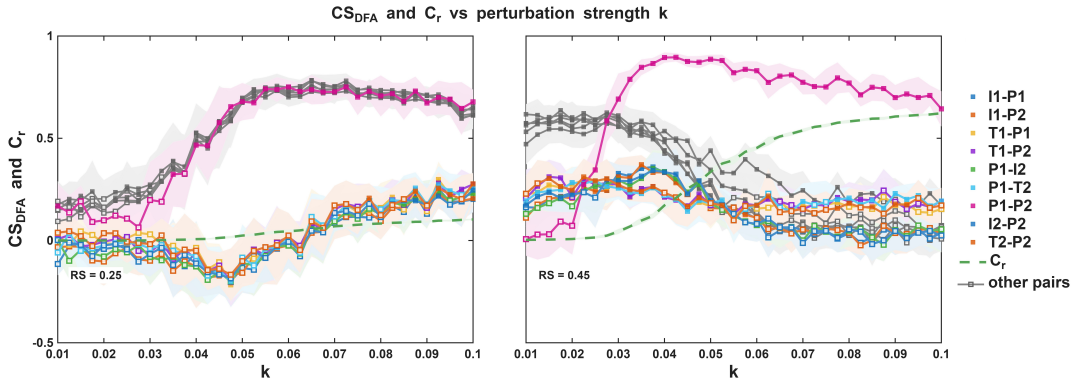


Figure 8. CS, computed using detrended fluctuation analysis (DFA), and cooperation rate (C_r) as functions of learning strength k of the SharePay thresholds. Panel (a) corresponds to $R = 0.25$ and panel (b) to $R = 0.45$. Colored curves represent CS between selected threshold pairs involving the payoff sharing thresholds, while gray curves denote other pairwise combinations. The dashed green curve indicates C_r. Shaded regions denote variability across ensembles.

a high-synchronization regime across multiple threshold pairs. The corresponding cooperation rate C_r increases with k and reaches substantially higher values in the high-R condition, co-occurring with the emergence of strong event-based CS.

The same analysis performed using DFA-based scaling (Fig. 8) captures changes in coordination, but with weaker resolution in the high-cooperation regime. DFA-based CS remains more variable and less sharply organized than MDEA-based CS, indicating that the event-based scaling measure provides a more resolved description of the cooperative regime in this model. This contrast is consistent with the preceding results showing that cooperation is more strongly aligned with synchronized event-driven restructuring than with synchronized persistence alone.

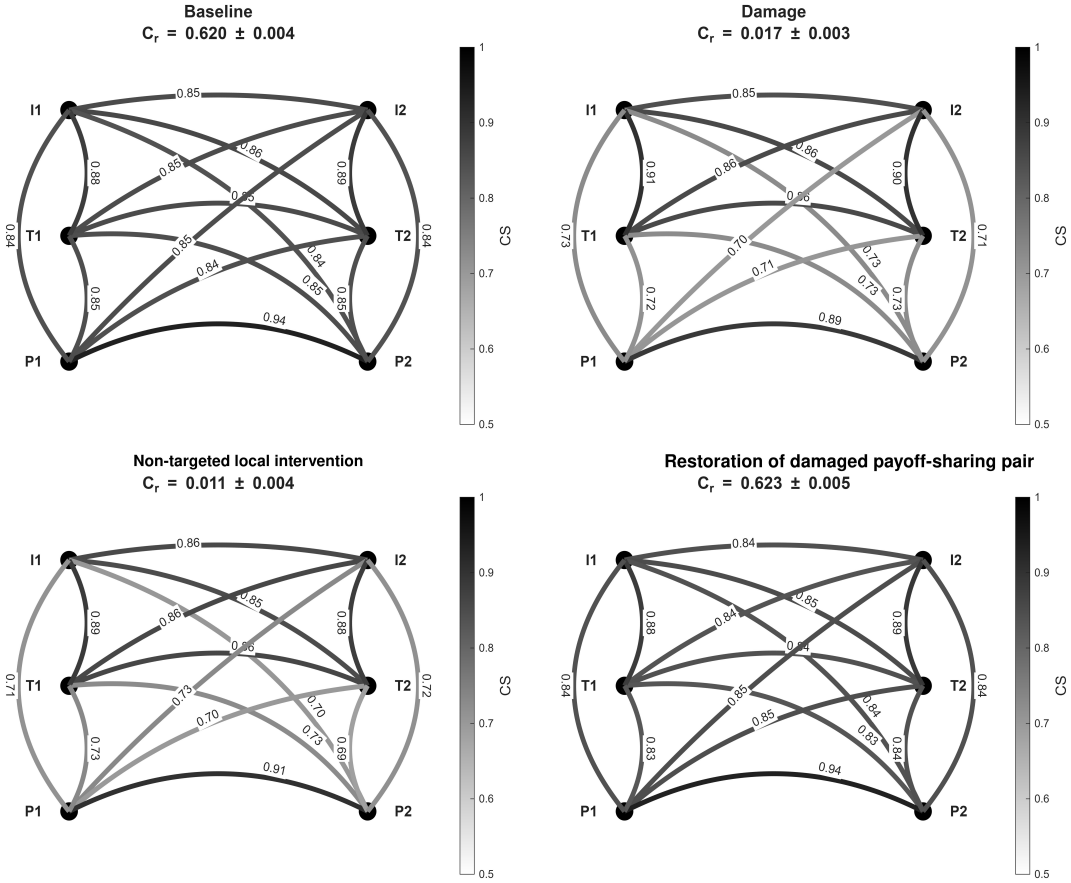


Figure 9. Complexity-synchronization (CS) networks under baseline, perturbation, and rescue conditions (MDEA, $R = 0.45$, ENS = 10). Graph representations of pairwise CS among the six adaptive thresholds ($I_1, T_1, P_1, I_2, T_2, P_2$), computed using modified diffusion entropy analysis (MDEA). Nodes correspond to threshold variables, and edges represent CS links. Edge thickness and grayscale intensity encode CS strength, dashed and solid edges retain the original nominal-p-value plotting convention and do not establish statistical significance, and edge labels report the corresponding CS values. Panels show (top left) baseline, (top right) perturbed (damage), (bottom left) non-targeted local rescue, and (bottom right) targeted rescue. The cooperation rate, C_r (mean ± SD across ensembles), is reported in each panel. The grayscale color bar spans CS values from 0.5 to 1.

CS describes changes accompanying perturbation We next examined changes in CS accompanying a predefined perturbation and its restoration. We damaged the system by reducing the learning increment of the payoff-sharing thresholds P_1 and P_2 from 0.1 to 0.025, while leaving the other adaptive thresholds unchanged. At $R = 0.45$, this perturbation reduced cooperation from the baseline level to a near-zero damaged state (Fig. 9). The CS network also changed, but the change was not a uniform collapse of all links. Instead, the damaged condition retained substantial synchronization while showing weakened links involving the payoff-sharing subsystem. This dissociation indicates that CS and cooperation measure different aspects of the dynamics: CS describes the organization of adaptive temporal structure, whereas C_r measures the behavioral function produced by that organization.

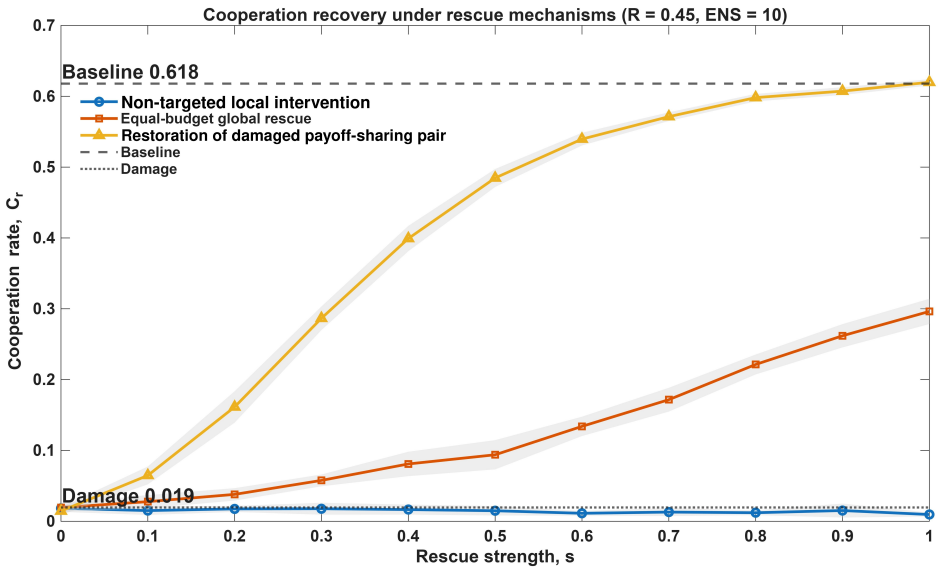


Figure 10. Cooperation recovery under different rescue strategies ($R = 0.45$, ENS $= 10$). Cooperation rate, C_r, is shown as a function of rescue strength, s, for three intervention strategies: non-targeted local rescue, equal-budget global rescue, and targeted intervention. Curves show the mean across ensembles, and shaded bands indicate $\pm$ SD. Horizontal dashed lines denote the baseline and perturbed (damage) levels.

targeted rescue restores cooperation To examine recovery from the specified perturbation, we compared three rescue strategies using the same damaged system. Non-targeted local rescue applied the intervention budget to a non-targeted pair, equal-budget global rescue distributed the budget across all thresholds, and targeted rescue restored the payoff-sharing predefined damaged pair. Figure 10 shows that targeted rescue recovered cooperation monotonically toward the baseline level as rescue strength increased. In contrast, non-targeted local rescue remained close to the damaged level, while equal-budget global rescue produced only partial recovery. Thus, restoration of the specific payoff-sharing subsystem was sufficient to recover cooperative performance, whereas non-specific interventions were inefficient under the same task conditions.

The same restoration protocol was examined in the low-R regime, where cooperation is weaker and DFA-based synchronization provides greater contrast for the relevant coordination structure. The corresponding DFA-based rescue networks and recovery curves are reported in Supplementary Information, Figs. S1 and S2. Together, the main and supplementary experiments show how CS network patterns evolve alongside cooperative recovery in two interaction regimes.

Supporting renewal-related analyses are reported in Supplementary Information, Figs. S4 and S5; their interpretation is discussed below as supporting mechanistic evidence rather than as the primary basis of the paper's central claim.

Discussion

Our results highlight a useful distinction between the coordination of observed variables and the coordination of their changing temporal statistics. The same six adaptive thresholds yield two different CS network descriptions. MDEA, which follows event-based diffusion scaling, reveals a positive relationship between CS and cooperation across the sensing-radius sweep. DFA, which measures fluctuation scaling in the original trajectories, reveals a negative relationship. The contrast is reproduced across ten stochastic ensembles and three representative pairs, with Holm-adjusted $p = 0.0084$ for each of the six slope tests. Thus, the estimator is not merely a technical choice: it shapes which aspect of adaptive coordination becomes visible.

This extends earlier physiological applications of CS[7,8] to a setting in which the underlying variables represent evolving decisions and the outcome is cooperative performance. Complexity matching concerns the similarity of scaling properties, whereas CS tracks the covariation of their changes[14,15]. Direct Pearson correlation of the thresholds provides another, complementary perspective (Supplementary Fig. S3). By comparing these representations in one adaptive model, we can begin to separate amplitude-level similarity from coordinated changes in temporal organization.

The perturbation experiments offer a second perspective. Weakening payoff-sharing learning reduces cooperation and reorganizes the CS network, while restoring those learning increments recovers performance and changes the network structure again. Under the equal-budget comparisons examined, direct restoration of the affected payoff-sharing channels produces greater recovery than either a selected unaffected-pair adjustment or a distributed adjustment. These experiments were deliberately constructed around a specified perturbation so that the relationship among adaptation, cooperative behavior, and network organization could be examined under controlled conditions. They illustrate a potential use of CS networks as interpretable descriptions of how a cooperative system responds to intervention.

The ensemble-level tests provide statistical support for the cooperation–CS slope contrast. The network maps and restoration curves serve a different purpose: they show the structure and evolution of coordination under defined model conditions. This combination of quantitative validation and controlled illustration makes the approach useful for generating more specific questions about coordination and recovery. A natural next step is to investigate how these network signatures behave in larger agent populations, under other learning rules, and in systems where the location of a perturbation is initially unknown.

The supporting event analyses offer a possible interpretation of the MDEA results. For the representative I_1 threshold, the aging comparison and inter-event autocorrelations suggest weaker interval memory in the higher-cooperation regime (Supplementary Figs. S4 and S5). At the finest stripe size, one fitted waiting-time exponent is near $\mu = 2$, compatible with $1/f$-like scaling under the relevant renewal assumptions[14]. These are illustrative analyses, not proof that every threshold or every CS pair follows a renewal process. They should not be used to infer a unique mechanism for the contrast with DFA.

These findings suggest a broader research direction: tracking CS networks as adaptive systems move between cooperative states, rather than reducing coordination to a single correlation or performance score. Testing the approach in additional agent models and experimental data would help determine which network signatures generalize across settings.

Conclusion

Complexity synchronization networks reveal complementary aspects of adaptive cooperation. In our predator–prey model, event-based MDEA and fluctuation-based DFA yield opposite, reproducible associations between CS and cooperative performance across ten stochastic ensembles (six Holm-adjusted tests, $p = 0.0084$). The accompanying perturbation and restoration experiments illustrate how network organization changes as cooperative function is disrupted and recovered. Together, these results provide a foundation for using time-varying scaling networks to study coordination, adaptation, and resilience in interacting systems.

Acknowledgements

Research was sponsored by the Army Research Laboratory and was accomplished under Cooperative Agreement Number W911NF-23-2-0162. The views and conclusions contained in this document are those of the authors and should not be interpreted as representing the official policies, either expressed or implied, of the Army Research Laboratory or the U.S. Government. The U.S. Government is authorized to reproduce and distribute reprints for Government purposes notwithstanding any copyright notation herein.

Author contributions

K.M. conceived the study, developed the model and analyses, and drafted the manuscript. All authors contributed to interpretation of the results, provided critical feedback, revised the manuscript, and approved the final version.

Competing interests

The authors declare no competing interests.

Data availability

All MATLAB codes used to generate the results of this study are publicly available at https://github.com/Koroshi137/Complexity-synchronization-networks-reveal-distinct-modes-of-coordination-in-a-predator-prey-model.git. The saved numerical results (.mat files) and corresponding plotting-only MATLAB scripts for the original figures are available together at https://drive.google.com/drive/folders/1nsBMYfHT2zdiWQ-1FdK4ke

kL1ljbBBH5?usp=sharing, allowing the manuscript figures to be reproduced without rerunning the computationally intensive stochastic simulations.

The ensemble-level slope validation outputs (CSV, PDF, and MDEA/DFA ensemble MAT files) are supplied with the Supplementary Information source package. The validation script is included in the accompanying reproducibility folder.

The ensemble-level validation CSV, MAT files, and MATLAB validation script are included in the accompanying Overleaf source archive.

Additional information

Supplementary material is provided in the accompanying Supplementary Information.

References

1. Axelrod, Robert; Hamilton, William D.. The evolution of cooperation. *Science*, 211, 1390–1396. (1981). doi:10.1126/science.7466396.
2. Nowak, Martin A.. Five rules for the evolution of cooperation. *Science*, 314, 1560–1563. (2006). doi:10.1126/science.1133755.
3. Strogatz, Steven H.. Sync: How Order Emerges from Chaos in the Universe, Nature, and Daily Life. *Hyperion*. (2003).
4. Pikovsky, Arkady; Rosenblum, Michael; Kurths, Jürgen. Synchronization: A Universal Concept in Nonlinear Sciences. *Cambridge University Press*. (2001).
5. Dumas, Guillaume; Nadel, Jacqueline; Soussignan, Robert; Martinerie, Jacques; Garnero, Line. Inter-brain synchronization during social interaction. *PLOS ONE*, 5, e12166. (2010). doi:10.1371/journal.pone.0012166.
6. Konvalinka, Ivana; Xygalatas, Dimitris; Bulbulia, Joseph; Schjødt, Uffe; Jegindø, Else-Marie; Wallot, Sebastian; Van Orden, Guy; Roepstorff, Andreas. Synchronized arousal between performers and related spectators in a fire-walking ritual. *Proceedings of the National Academy of Sciences*, 108, 8514–8519. (2011). doi:10.1073/pnas.1016955108.
7. Mahmoodi, Korosh; Kerick, Scott E.; Grigolini, Paolo; Franaszczuk, Piotr J.; West, Bruce J.. Complexity synchronization: a measure of interaction between the brain, heart and lungs. *Scientific Reports*, 13, 11433. (2023).
8. West, Bruce J.; Grigolini, Paolo; Kerick, Scott E.; Franaszczuk, Piotr J.; Mahmoodi, Korosh. Complexity synchronization of organ networks. *Entropy*, 25, 1393. (2023).
9. Mahmoodi, Korosh; West, Bruce J.; Grigolini, Paolo. Self-organizing complex networks: individual versus global rules. *Frontiers in Physiology*, 8, 478. (2017).
10. Mahmoodi, Korosh; West, Bruce J.; Gonzalez, Cleotilde. Selfish algorithm and emergence of collective intelligence. *Journal of Complex Networks*, 8, cnaa019. (2020).
11. Liu, Yang-Yu; Slotine, Jean-Jacques; Barabási, Albert-László. Controllability of complex networks. *Nature*, 473, 167–173. (2011). doi:10.1038/nature10011.
12. Cornelius, Sean P.; Kath, William L.; Motter, Adilson E.. Realistic control of network dynamics. *Nature Communications*, 4, 1942. (2013). doi:10.1038/ncomms2939.
13. Gao, Jianxi; Barzel, Baruch; Barabási, Albert-László. Universal resilience patterns in complex networks. *Nature*, 530, 307–312. (2016). doi:10.1038/nature16948.
14. Aquino, Gerardo; Bologna, Mauro; West, Bruce J.; Grigolini, Paolo. Transmission of information between complex systems: 1/f resonance. *Physical Review E*, 83, 051130. (2011).
15. West, Bruce J.; Geneston, Elvis L.; Grigolini, Paolo. Maximum information exchange between complex networks. *Physics Reports*, 468, 1–99. (2008).

Supplementary Files

This is a list of supplementary files associated with this preprint. Click to download.

- SupplementaryInformationforComplexitysynchronizationnetworksrevealdistinctmodesofcoordinationinanadaptivepredatorpreymodel.pdf